Supporting Information

Surmounting Instability of Atomically Precise Metal Nanoclusters Towards Boosted Photoredox Organic Transformation

Yu-Bing Li, Fang-Xing Xiao*

College of Materials Science and Engineering, Fuzhou University, Fuzhou, Fujian 350108, P.R. China.

Email: fxxiao@fzu.edu.cn

Table of Contents

Page NO.

Experimental section

S1. Materials

Deionized water (DI H_2O, Millipore, 18.2 MΩ·cm resistivity), graphite sheets (50 mm × 20 mm × 0.1 mm, 99.6%), ethylene glycol $(CH_2OH)_2$, ammonium fluoride (NH_4F), hydrogen fluoride (HF), nitric acid (HNO_3), tetraoctylammonium bromide (TOAB), toluene, sodium borohydride ($NaBH_4$), 4-dimethylaminopyridine (DMAP, $C_7H_{10}N_2$), sulfuric acid (H_2SO_4), sodium hydroxide (NaOH), *L*-glutathione (reduced, 98%, Sigma-Aldrich), gold (III) chloride trihydrate (99.9%, Sigma-Aldrich), Methanol (CH_3OH), Ethanol (C_2H_6O), Ethylene glycol ($C_2H_6O_2$), Glycerol ($C_3H_8O_3$), Lactic acid ($C_3H_6O_3$), Sodium sulfate (Na_2SO_4). All the materials are analytical grade and used as received without further purification.

S2. Preparation of CdS NWs[1]

1.124 g of cadmium diethyldithiocarbamate ($Cd(S_2CNEt_2)_2$), prepared by precipitation from a stoichiometric mixture of sodium diethyldithiocarbamate trihydrate and cadmium chloride in deionized water (DI H_2O), was added to a Teflon-lined stainless steel autoclave with a capacity of 50 mL. Then, the autoclave was filled with 40 mL of ethylenediamine to 80 % of the total volume. The autoclave was maintained at 453 K for 24 h and then allowed to cool to room temperature. A yellowish precipitate was collected and washed with absolute ethanol and DI H_2O to remove residue of organic solvents. The final products were dried in an oven at 333 K for 12 h.

S3. Preparation of $Au_{25}(GSH)_{18}$ NCs[2]

Glutathione-protected $Au_{25}(GSH)_{18}$ NCs was prepared according to the previous method previously reported with some modifications. Briefly, glutathione (reduced form, 1 mmol) was added to methanol (50 mL) containing $HAuCl_4 \cdot 3H_2O$ (0.25 mmol). Under vigorous stirring, an ice-cold $NaBH_4$ aqueous solution (0.2 M, 12.5 mL) was added and aged for 1 h. The obtained precipitate was thoroughly washed with methanol and dried in vacuum at room temperature to obtain a mixture of Au NCs. The mixture (4.9 mg) was dissolved in an aqueous solution (7 mL) containing glutathione (130.7 mg) and stirred at 55 ^oC under air bubbling for 6-9 h to obtain $Au_{25}(GSH)_{18}$ NCs. To remove excess glutathione, the obtained solution containing the $Au_{25}(SG)_{18}$ NCs was loaded into a dialysis membrane (MWCO 8000) and stirred slowly at <10 ^oC for 12 h. The precipitate formed during the dialysis was removed with a filter (pore size, 0.2 μm). It was confirmed by polyacrylamide gel electrophoresis that the obtained solution contains no other clusters.

S4. Modification of CdS NWs surface

0.1 g CdS NWs was first dispersed in 100 mL of DI water by sonication for 10 min. Then, 9 mL of 1.0 mol L^{-1} 2-mercaptoethylamine (MEA) was added under vigorous stirring (1000 rpm). The CdS NWs reacted with the modifier for 1 h at room temperature. Finally, the modified CdS/MEA NWs samples were sufficiently rinsed with ethanol to wash away any remaining modifier moiety, and fully dried at 333 K in an oven.

S5. Preparation of CdS/$Au_{25}(GSH)_{18}$ NCs heterostructure (self-assembly)

0.1 g modified CdS@MEA NWs was dispersed in 5 mL of $Au_{25}(GSH)_{18}$ NCs (the weight ratio of 5%) solution and stirred for 10 min. Then, different amounts of $Au_{25}(GSH)_{18}$ NCs were added into modified CdS@MEA NWs dispersion under vigorous stirring (1000 rpm). After mixing for 10 min, the mixture was centrifuged and washed with DI H_2O and fully dried at 333 K in an oven to obtain the final CdS/Au_{25}@GSH_{18} composites with 5% weight ratio of $Au_{25}(GSH)_{18}$ NCs.

S6. Determining the energy levels of $Au_{25}(GSH)_{18}$ NCs[3]

Cyclic voltammetry (CV) measurements were conducted using a three-electrode system, consisting of a glassy carbon disk as the working electrode, platinum gauze as the counter electrode, and an Ag/AgCl (0.54 V vs. RHE) as the reference electrode. The electrolyte solution was 0.1 M tetraethylammonium perchlorate (TEAP) in acetonitrile (C_2H_3N), which was purged with N_2 in a sealed vial for 10 min before use. CV curves were obtained by sweeping at 0.1 V s^{-1} in a mixed C_2H_3N/TEAP (0.1 M) solution, with the addition of 800 or 1000 μL of Au_{25}@GSH_{18} NCs.

S7. Preparation of working electrode[4]

Working electrodes were fabricated on FTO glass substrates that were first cleaned by sonication in ethanol for 30 minutes and then dried at 353 K. Scotch tape was used to protect the edges of the FTO glass. A 5 mg sample was dispersed in 0.5 mL of absolute ethyl alcohol by sonication to form a slurry, which was uniformly spread onto the pretreated FTO glass. After allowing it to dry in air, the Scotch tape was removed, and the uncoated part of the electrode was covered with nail polish. The exposed area of the working electrode was 1 cm^2.

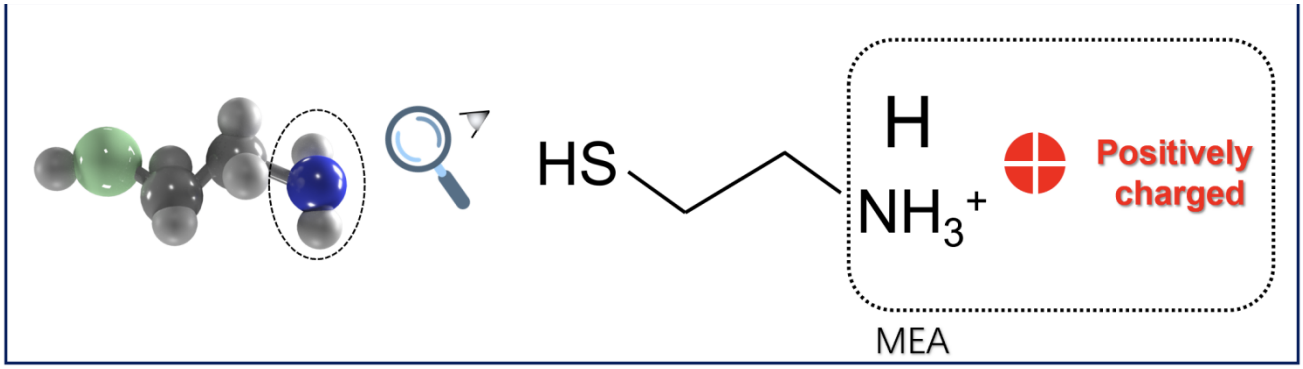

Fig. S1. Schematic model and molecular structure of MEA.

Note: The MEA molecule contains both a thiol group (-SH) and an amino group ($-NH_2$). At a neutral pH of 7, the amino group tends to accept a proton (H^+), forming an ammonium ion ($-NH^{3+}$), thus producing the positively charged molecular.

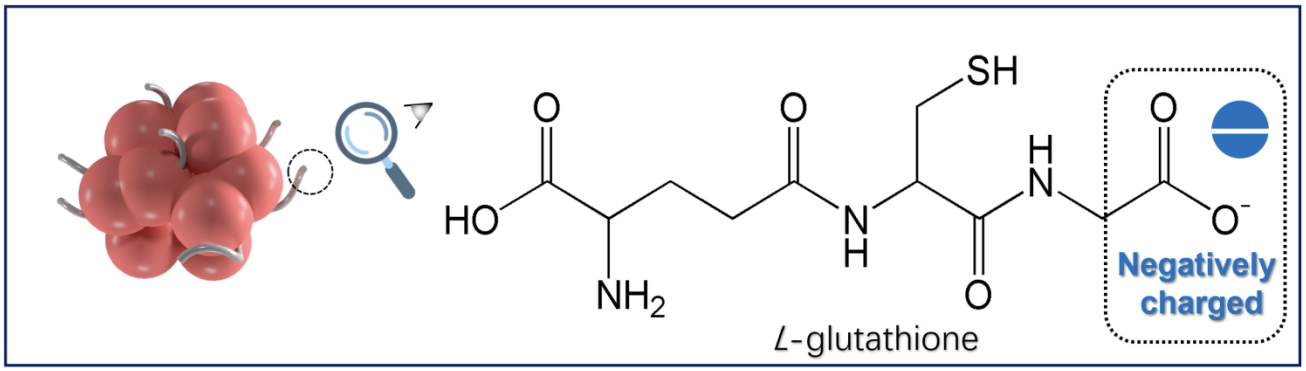

Fig. S2. Schematic model and molecular structure of GSH ligand.

Note: GSH ligands capped on the Au_x@GSH NCs surface provide various polar functional groups including carboxyl (-COOH), amino (-NH_2), and amide (-CONH-) groups, among which deprotonated -COO^- specie endows Au_x@GSH NCs with negatively charged surface that is beneficial for interaction with the MEA-modified positively charged CdS for electrostatic self-assembly buildup.

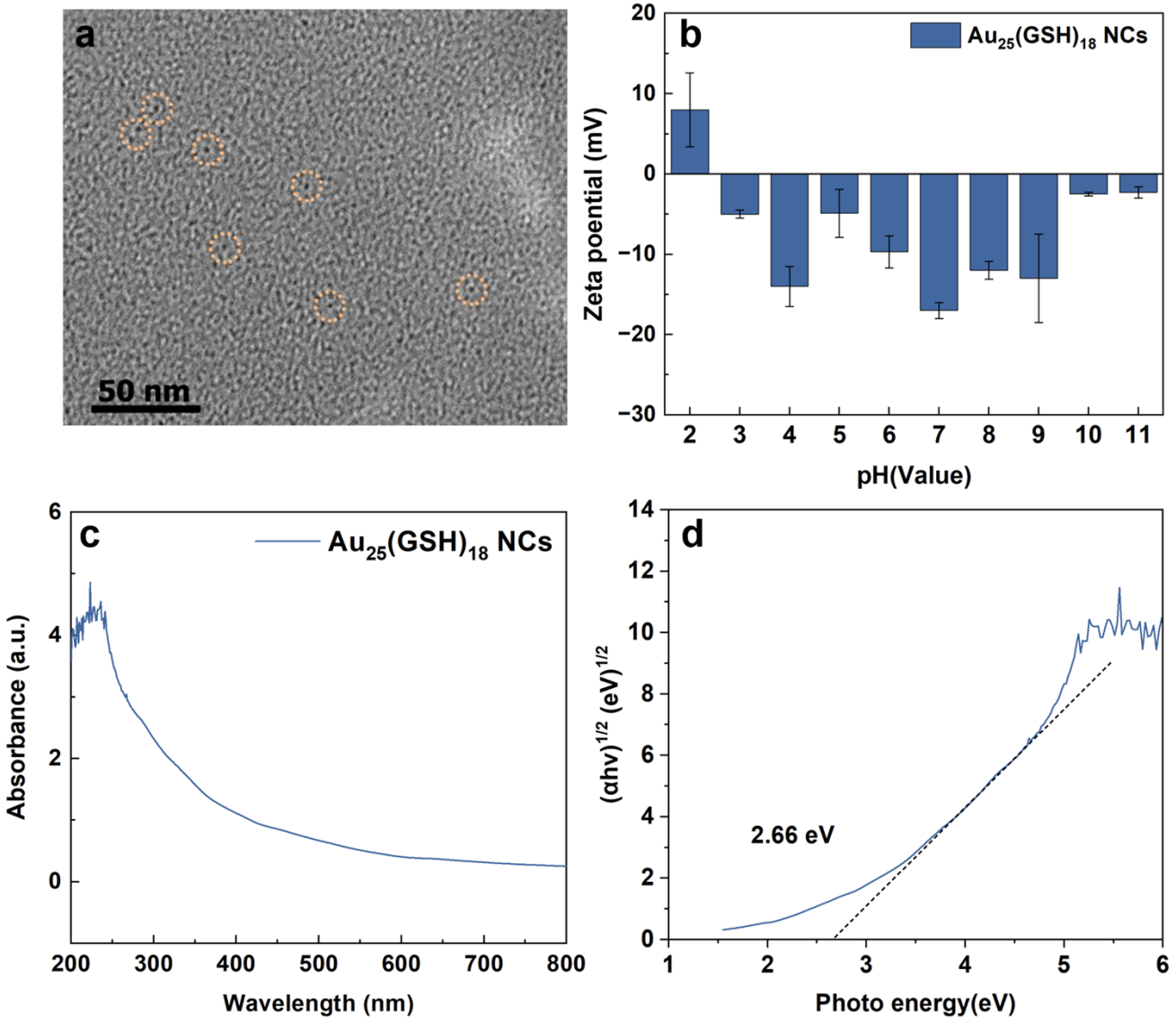

Fig. S3. (a) TEM image, (b) zeta potentials, (c) UV-vis absorption spectrum of $Au_{25}(GSH)_{18}$ NCs aqueous solution with (d) bandgap determination. TEM image shown is cited from ***J. Am. Chem. Soc. 2020, 142, 52, 21899–21912.***[5]

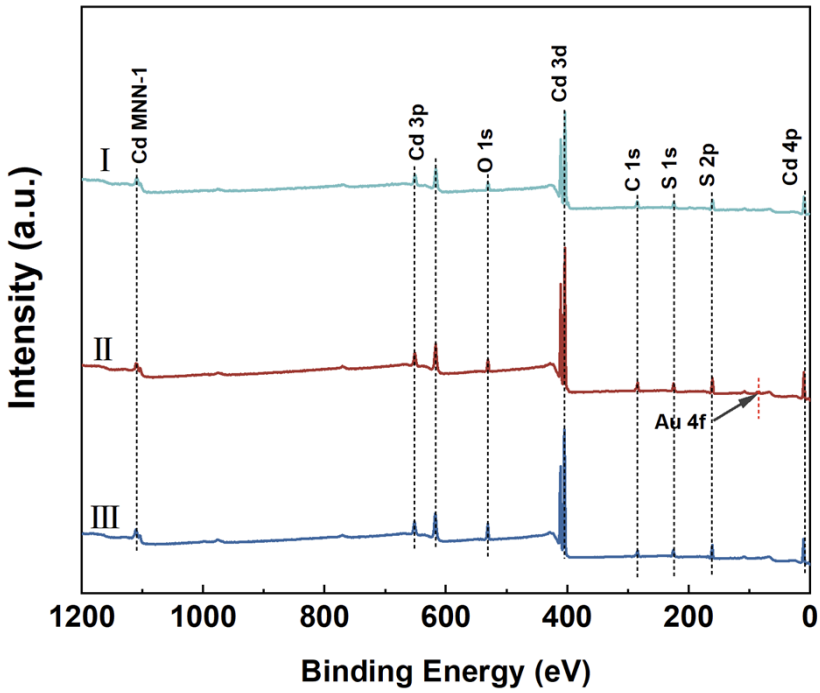

Fig. S4. Survey spectra of (I) CdS NWs, (II) CdS/$Au_{25}(GSH)_{18}$ and (III) CdS/Au heterostructures.

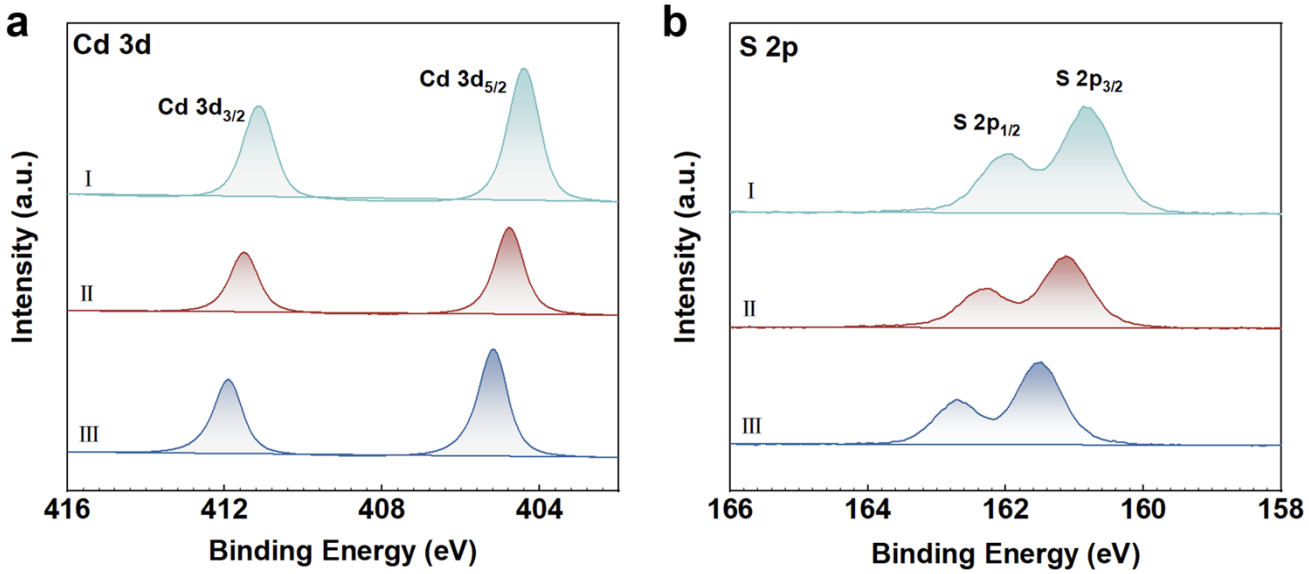

Fig. S5. High-resolution (a) Cd 3d and (b) S 2P spectra of (I) CdS NWs, (II) CdS/$Au_{25}(GSH)_{18}$ and (III) CdS/Au heterostructures.

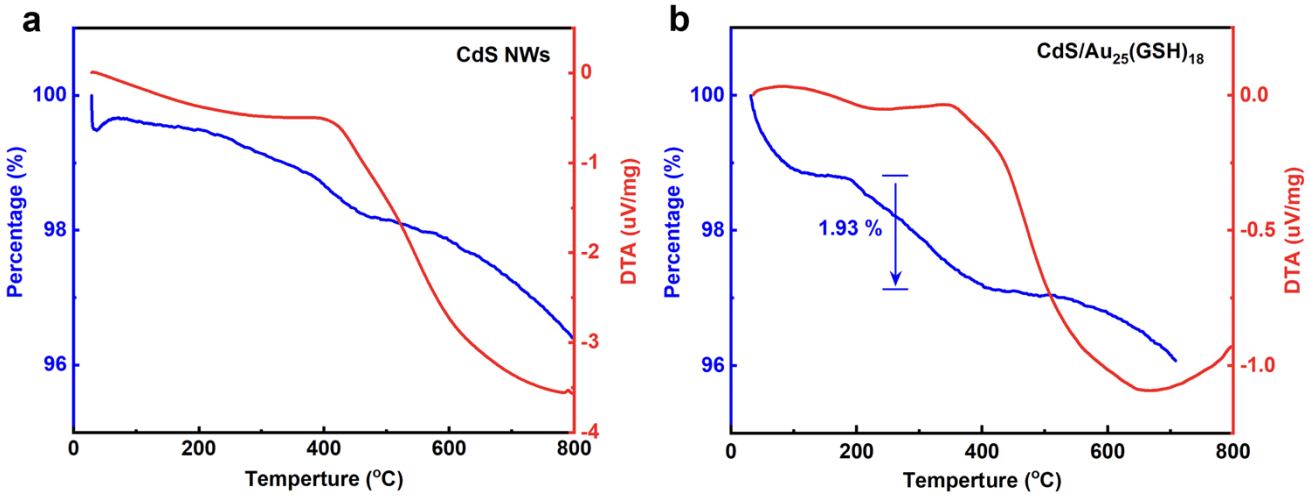

Fig. S6. TG results of CdS NWs and CdS/$Au_{25}(GSH)_{18}$ heterostructure.

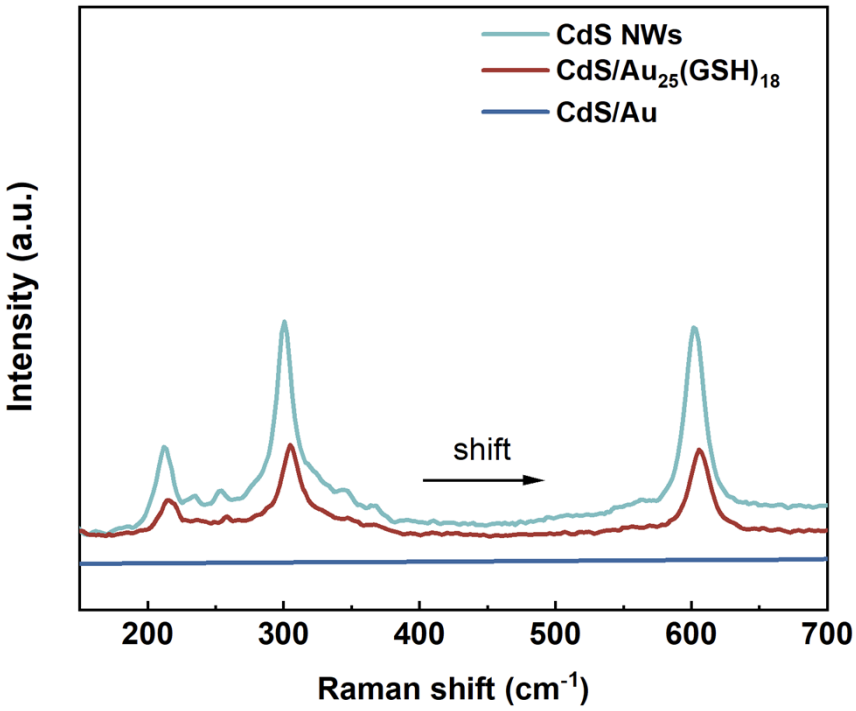

Fig. S7. Raman spectra of CdS NWs, $CdS/Au_{25}(GSH)_{18}$ and CdS/Au heterostructure.

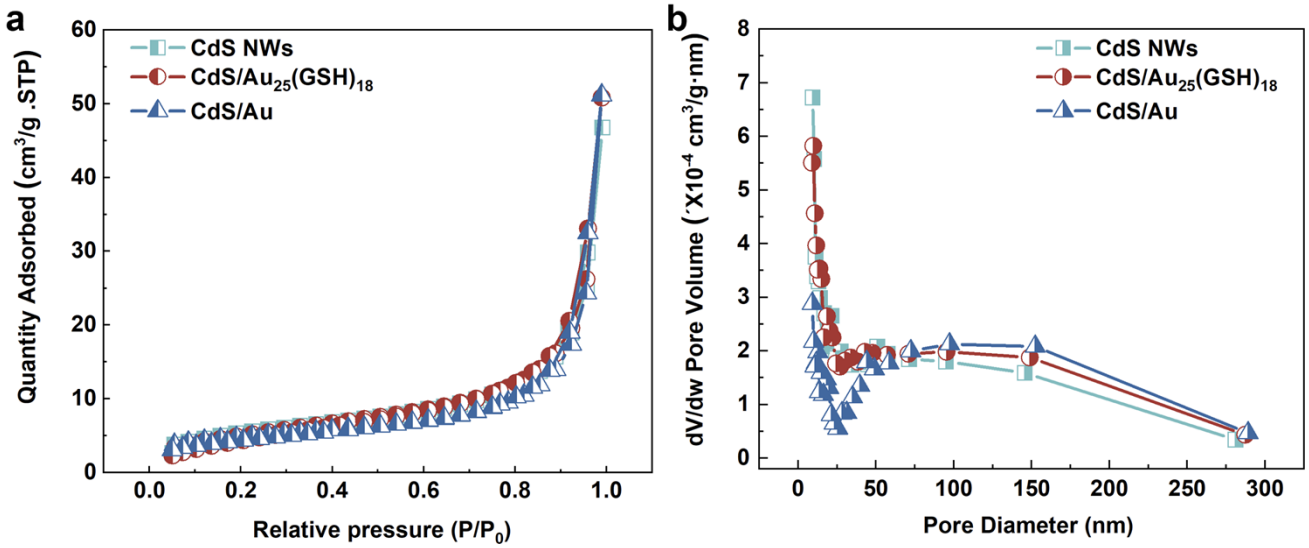

Fig. S8. (a) Nitrogen adsorption-desorption isotherms of blank CdS NWs, $CdS/Au_{25}(GSH)_{18}$ and CdS/Au heterostructures with the corresponding (b) pore size distribution plots.

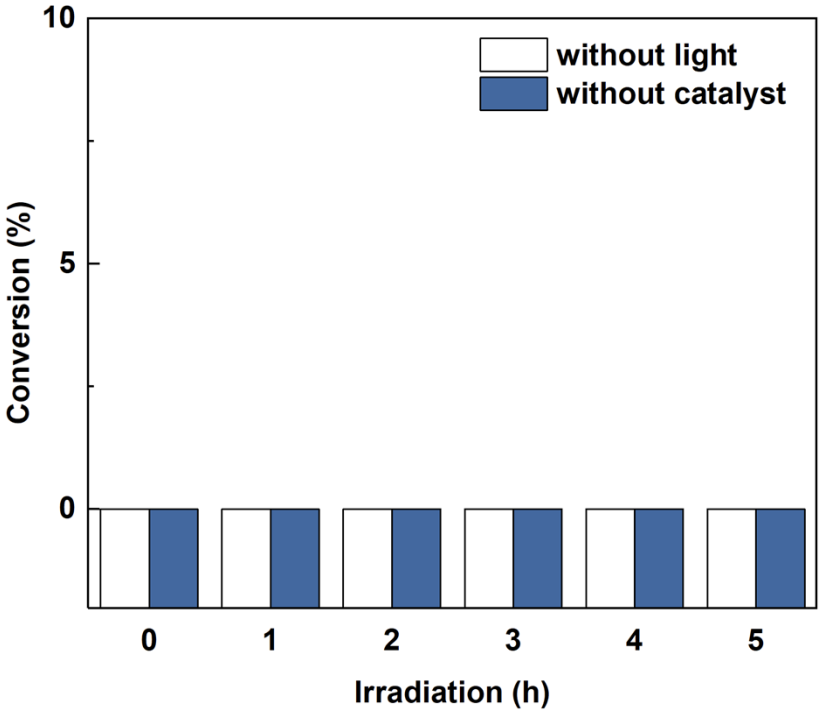

Fig. S9. Blank experiments for photocatalytic reduction of 4-NA without light irradiation or without adding photocatalyst.

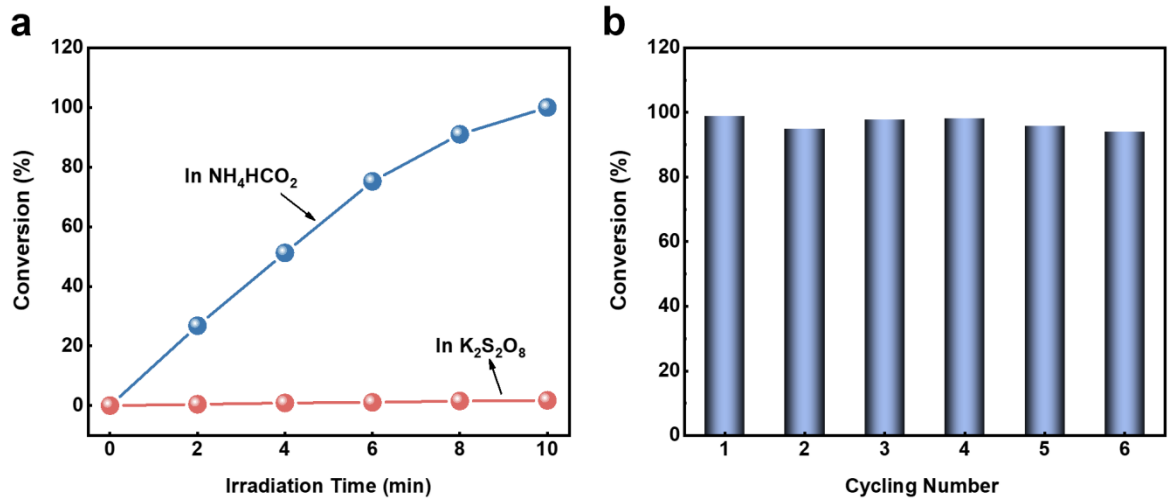

Fig. S10. Control experiments with the addition of $K_2S_2O_8$ as electron scavenger, (b) cyclic photoreduction of 4-NA over CdS/Au heterostructure under visible light irradiation ($\lambda > 420$ nm).

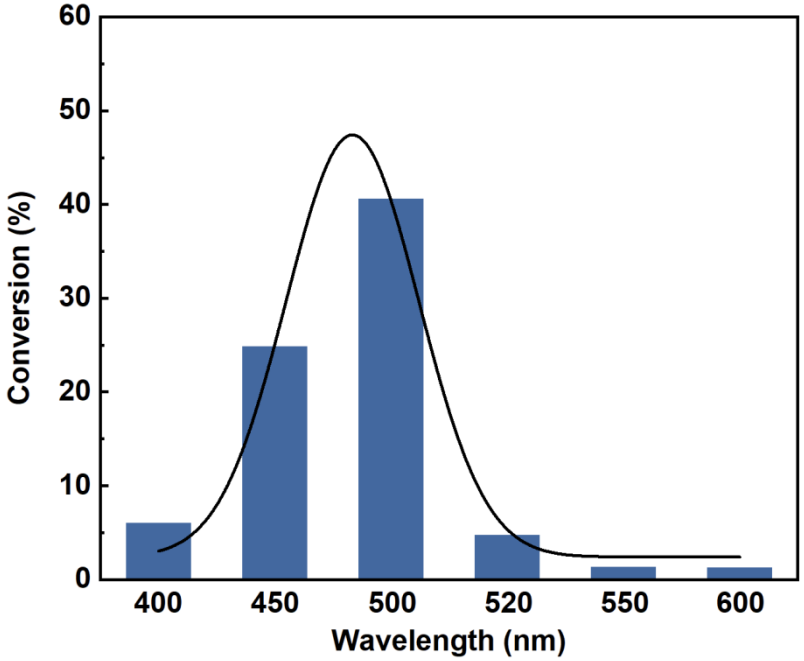

Fig. S11. Action spectrum of CdS/Au heterostructure under monochromatic light irradiation toward 4-NA photoreduction.

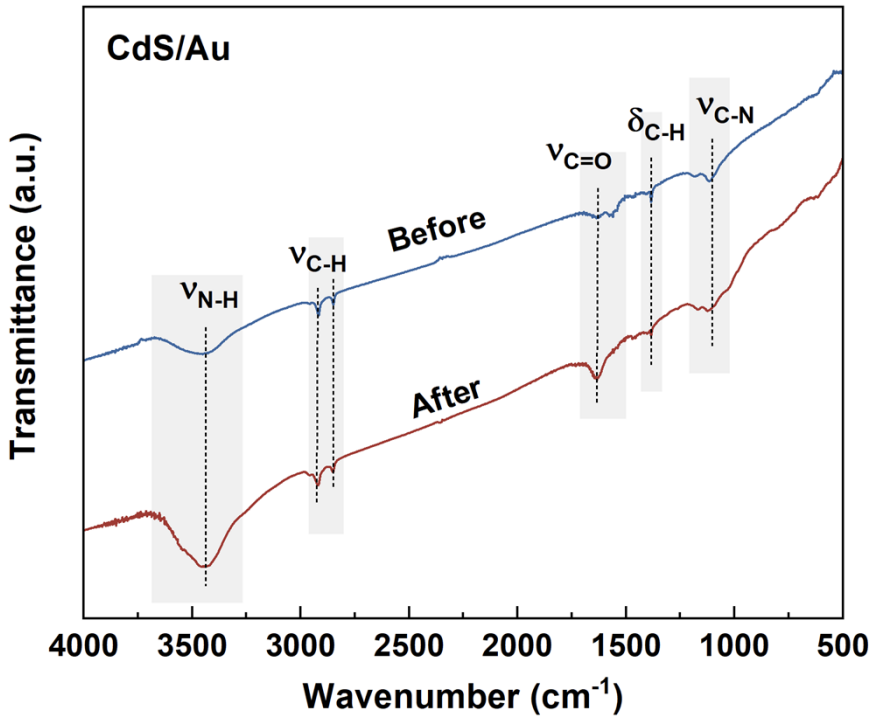

Fig. S12. FTIR spectra of CdS/Au heterostructure before and after cyclic photoreduction of 4-NA under visible light irradiation (8 h, $\lambda > 420$ nm).

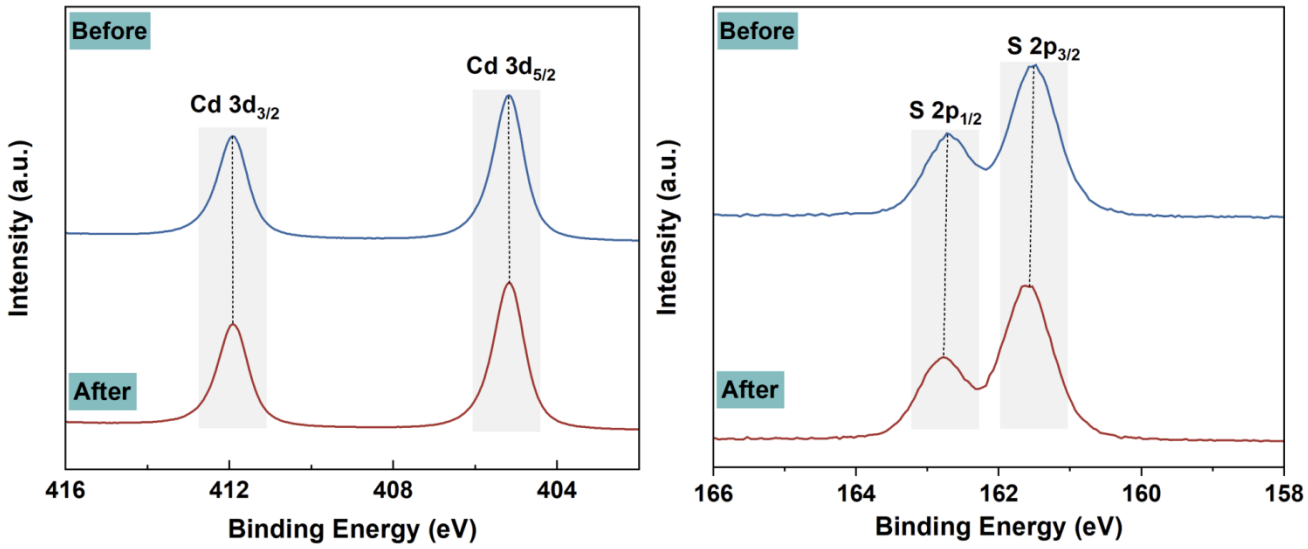

Fig. S13. High-resolution Cd 3d and S 2P spectra of CdS/Au heterostructures before and after cyclic photoreduction of 4-NA under visible light irradiation (8 h, $\lambda > 420$ nm).

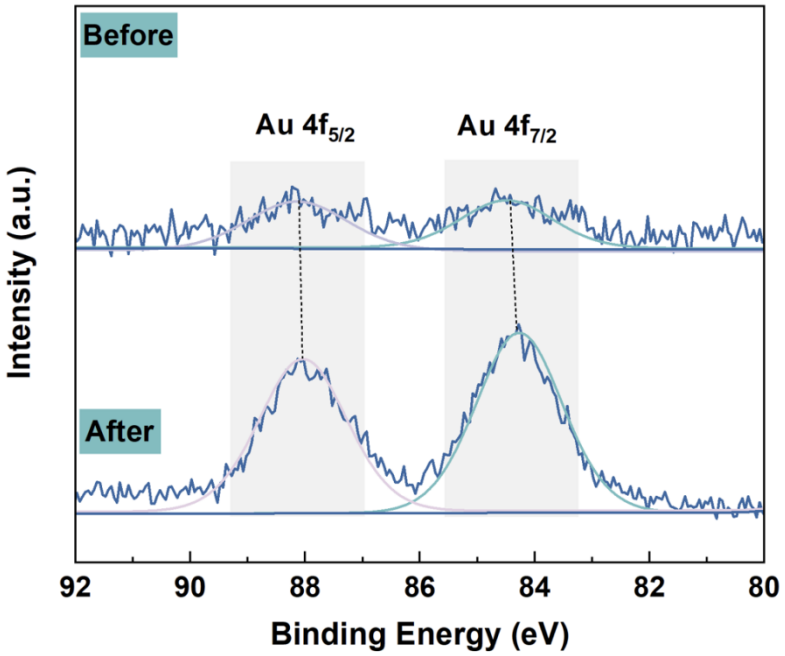

Fig. S14. High-resolution Au 4f spectra of CdS/Au before and after cyclic photoreduction of 4-NA under visible light irradiation (8 h, $\lambda > 420$ nm).

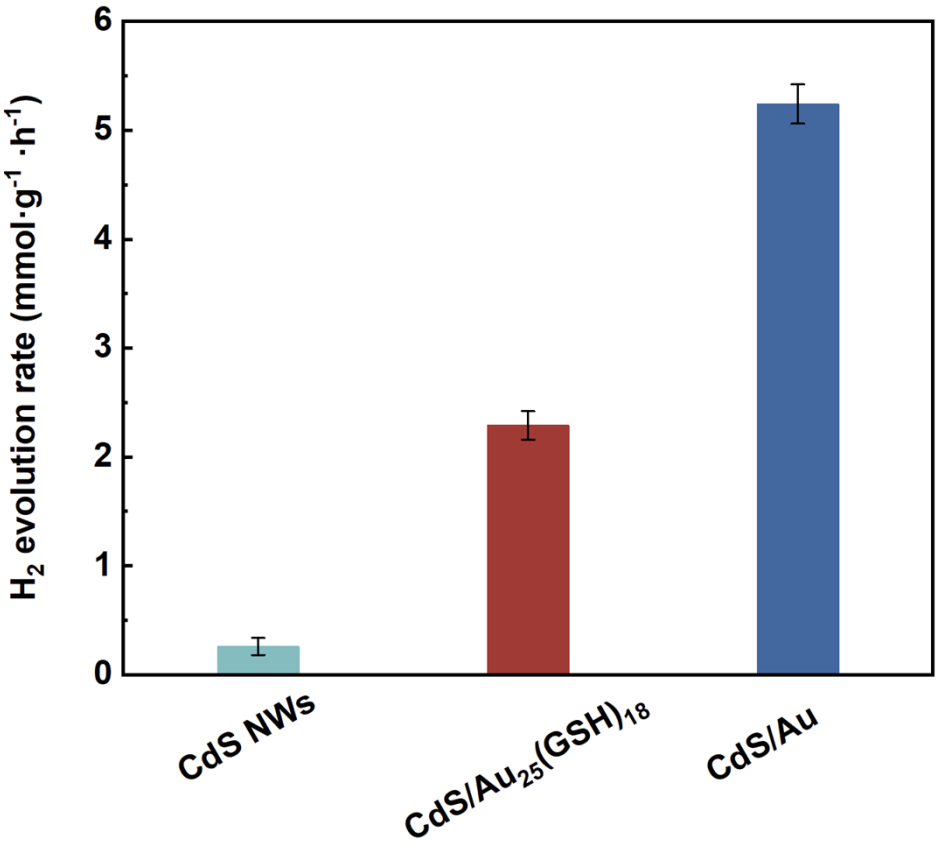

Fig. S15. Photocatalytic H_2 evolution rates of CdS NWs, $CdS/Au_{25}(GSH)_{18}$ and CdS/Au heterostructure under visible light irradiation ($\lambda > 420$ nm).

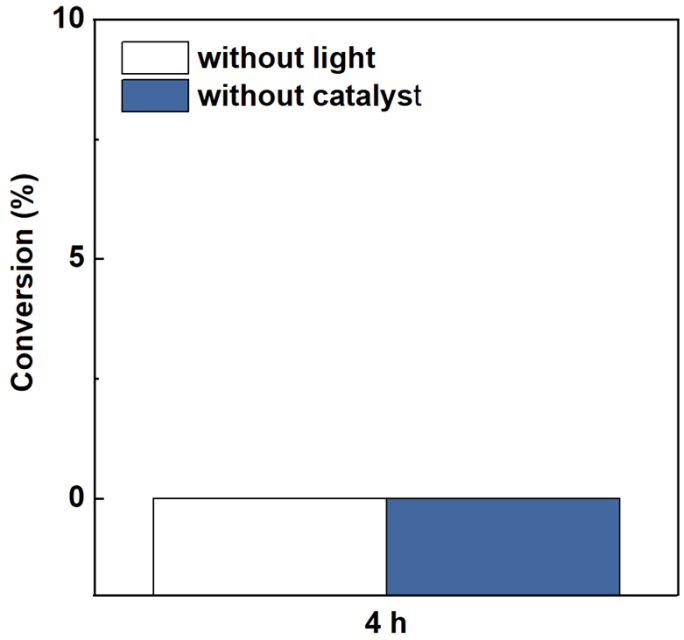

Fig. S16. Blank experiments for photocatalytic selective oxidation of benzyl alcohol without light or without adding photocatalyst.

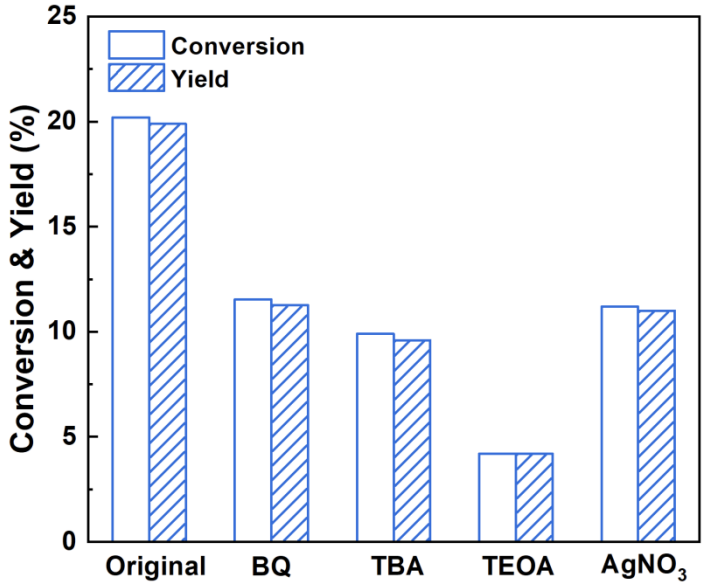

Fig. S17. Photocatalytic selective oxidation of benzyl alcohol over CdS/Au for 4 h by adding BQ, TBA, TEOA and $AgNO_3$ as scavengers for quenching superoxide radical ($O_2^{\cdot -}$), hydroxyl radical ($OH^{\cdot}$), holes (h^+) and electrons (e^-), respectively.

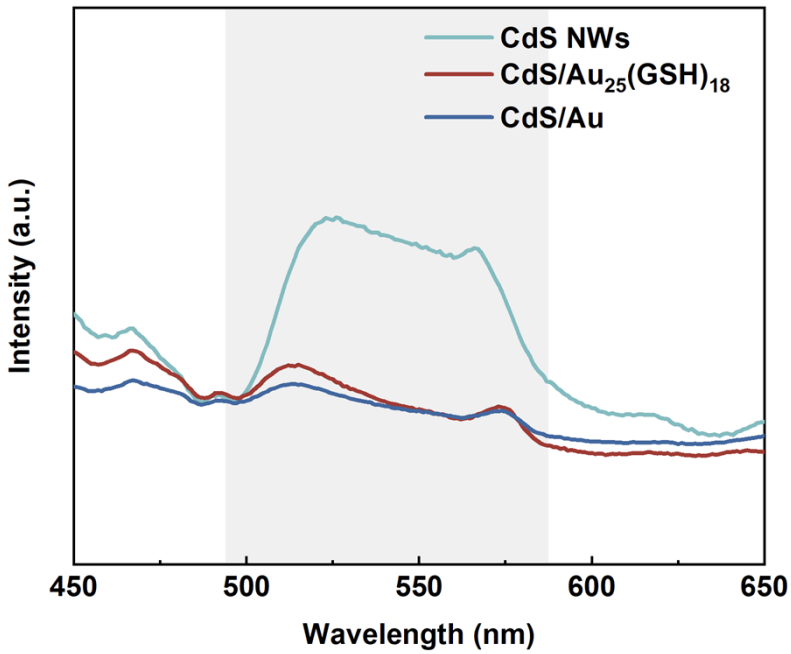

Fig. S18. PL spectra of different samples with an excitation wavelength of 350 nm.

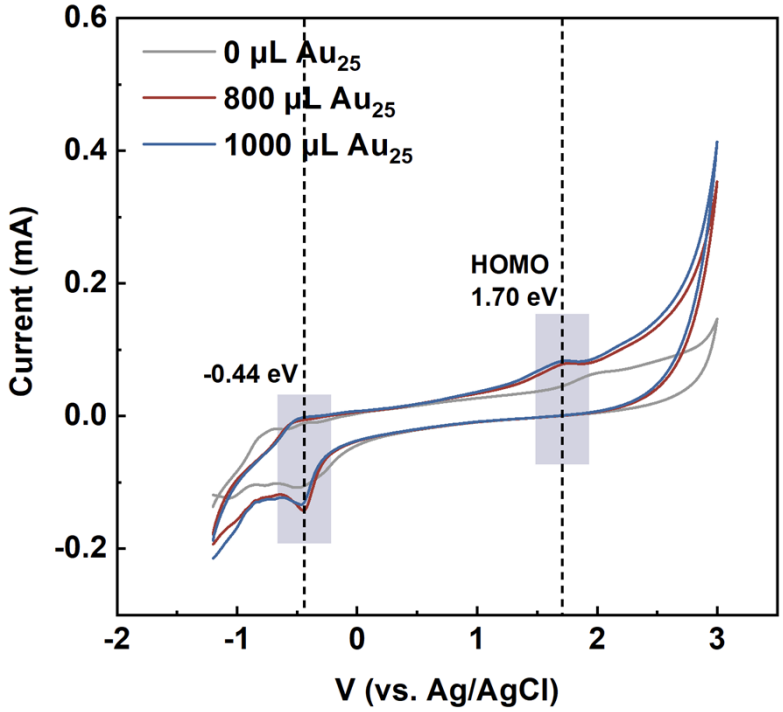

Fig. S19. CV curves of $Au_{25}(GSH)_{18}$ NCs (electrolyte: degassed acetonitrile containing 0.1 mol L^{-1} TEAP).

Note: CV curve of $Au_{25}(GSH)_{18}$ NCs shows an oxidation potential at 1.90 V (vs. NHE). Considering the bandgap of $Au_{25}(GSH)_{18}$ NCs (2.66 eV, **Fig. S3d**), LUMO level of $Au_{25}(GSH)_{18}$ NCs is determined to be - 0.76 eV (vs. NHE). Thus, electrons photoexcited over $Au_{25}(GSH)_{18}$ NCs can flow from the LUMO level to the CB of CdS (-0.45 V vs. NHE) in terms of favorable energy level alignment.

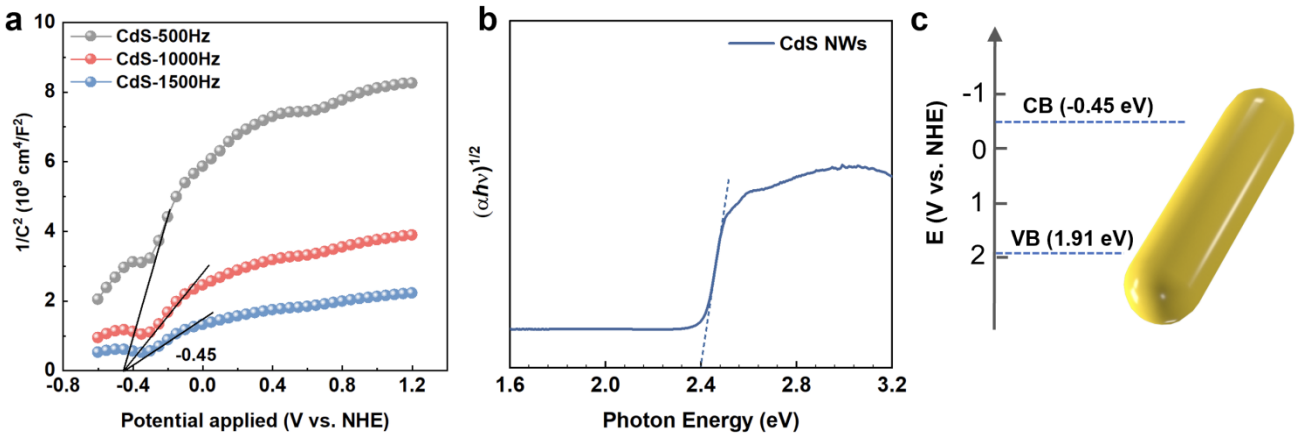

Fig. S20. (a) Mott-Schottky plots of CdS NWs probed under different frequencies, (b) DRS result with transformed plots based on the Kubelka-Munk function vs. the energy of light and (c) energy level position of CdS NWs.

Table S1. Peak position with corresponding functional groups.

Peak position (cm^{-1})	***Vibration mode***
3439.7	N-H stretching vibration[6]
2919.5	C-H stretching vibration[7]
2850.2	C-H stretching vibration[7]
1633.9	C=O stretching vibration[5]
1466.8	C-H stretching vibration[1]
1377.8	C-H stretching vibration[1]
1038.6	C-N stretching vibration[8]

Table S2. Chemical bond species vs. B.E. for different samples.

Element	*CdS*	*CdS/Au$_{25}$(GSH)$_{18}$*	*CdS/Au*	*Chemical Bond Species*
C 1s A	284.78	284.81	284.80	C-C/C-H[6]
C 1s B	285.68	286.44	286.74	C-OH/C-O-C
C 1s C	287.94	288.75	288.26	Carboxylate (CO_3^{2-})[3]
N 1s	/	399.57	/	-NH_2/-NH-[6]
Cd 3d$_{5/2}$	404.41	404.78	405.19	Cd^{2+}[9]
Cd 3d$_{3/2}$	411.13	411.51	411.90	Cd^{2+}
S 2p$_{3/2}$	160.82	161.11	161.49	S^{2-}[1]
S 2p$_{1/2}$	161.96	162.31	162.68	S^{2-}
Au 4f$_{7/2}$	N.D.	84.43	84.47	Metallic Au[05]
Au 4f$_{5/2}$	N.D.	88.10	88.07	Metallic Au^0
Au 4f$_{7/2}$	N.D.	85.49	/	Au^{+2}
Au 4f$_{5/2}$	N.D.	89.02	/	Au^+

N.D.: Not Detected.

Table S3. Summary of the specific surface area, pore volume and pore size of CdS NWs, $CdS/Au_{25}(GSH)_{18}$ and CdS/Au heterostructures.

Samples	S_{BET} $(m^2 g^{-1})^a$	Total pore volume $(cm^3 g^{-1})^b$	Average pore size $(nm)^c$
CdS NWs	19.55	0.034	6.87
$CdS/Au_{25}(GSH)_{18}$	18.60	0.035	7.53
CdS/Au	16.32	0.032	7.75

[a] BET surface area is calculated from the linear part of the BET plot.

[b] Single point total pore volume of the pores at P/P0 = 0.99.

[c] Adsorption average pore width (4V/A by BET).

References

1. Y.-B. Li, T. Li, X.-C. Dai, M.-H. Huang, Y. He, G. Xiao and F.-X. Xiao, Cascade charge transfer mediated by in situ interface modulation toward solar hydrogen production, *J. Mater. Chem. A*, 2019, **7**, 8938-8951.
2. X. Yan, X.-Y. Fu and F.-X. Xiao, Filling the Gap: Atomically Precise Metal Nanoclusters-Induced Z-Scheme Photosystem toward Robust and Stable Solar Hydrogen Generation, *Adv. Funct. Mater.*, 2023, **33**, 2303737.
3. Y.-B. Li and F.-X. Xiao, Tuning the photosensitization efficiency of atomically precise metal nanoclusters by super-efficient and exquisite interface modulation, *J. Mater. Chem. A*, 2023, **11**, 589-599.
4. M.-H. Huang, X.-C. Dai, T. Li, Y.-B. Li, Y. He, G. Xiao and F.-X. Xiao, Stimulating Charge Transfer Over Quantum Dots via Ligand-Triggered Layer-by-Layer Assembly toward Multifarious Photoredox Organic Transformation, *J. Phys. Chem. C*, 2019, **123**, 9721-9734.
5. Z.-Q. Wei, S. Hou, X. Lin, S. Xu, X.-C. Dai, Y.-H. Li, J.-Y. Li, F.-X. Xiao and Y.-J. Xu, Unexpected Boosted Solar Water Oxidation by Nonconjugated Polymer-Mediated Tandem Charge Transfer, *J. Am. Chem. Soc.*, 2020, **142**, 21899-21912.
6. Y.-B. Li, T. Li, X.-C. Dai, M.-H. Huang, S. Hou, X.-Y. Fu, Z.-Q. Wei, Y. He, G. Xiao and F.-X. Xiao, Precise Tuning of Coordination Positions for Transition-Metal Ions via Layer-by-Layer Assembly To Enhance Solar Hydrogen Production, *Acs Appl. Mater. Interfaces*, 2020, **12**, 4373-4384.
7. T. Li, M.-H. Huang, Y.-B. Li, X.-C. Dai, Y. He, G. Xiao and F.-X. Xiao, General self-assembly of metal/metal chalcogenide heterostructures initiated by a surface linker: modulating tunable charge flow toward versatile photoredox catalysis, *J. Mater. Chem. A*, 2019, **7**, 21182-21194.
8. X.-Y. Fu, Z.-Q. Wei, S. Xu, X. Lin, S. Hou and F.-X. Xiao, Maneuvering intrinsic instability of metal nanoclusters for boosted solar-powered hydrogen production, *J. Phys. Chem. Lett.*, 2020, **11**, 9138-9143.
9. K. Wang, X.-Z. Ge, Q.-L. Mo, X. Yan, Y. Xiao, G. Wu, S.-R. Xu, J.-L. Li, Z.-X. Chen and F.-X. Xiao, Steering bi-directional charge transfer via non-conjugated insulating polymer, *J. Catal.*, 2022, **416**, 92-102.